Electrochimica Acta 441 (2023) 141791

Contents lists available at ScienceDirect

Electrochimica Acta

journal homepage: www.journals.elsevier.com/electrochimica-acta

Ethanol formation via CO_2 electroreduction at low overvoltage over exposed (111) plane of CuO thin film

Shikha Dhakar [a], Jatin Nama [1,a], Varsha Kumari [1,a], Rudranarayan Khatua [1,a], Anirban Mondal [a,3], Sudhanshu Sharma [*,a,2]

[a] Department of Chemistry, Indian Institute of Technology Gandhinagar, Gandhinagar 382355, Gujarat, India

ARTICLE INFO

Keywords:
CuO thin film
Sol-gel
Spin coating method
Gas chromatography
Electro-reduction
Bulk material

ABSTRACT

In this study, we fabricated CuO thin films using the sol-gel spin coating method. The fabricated thin films were utilized for electrocatalytic reduction of CO_2 (CO_2ER). Fabrication of thin film is vital to provide a large surface area and a more exposed (111) crystal plane for ethanol selectivity. This is verified by comparing it with bulk powder material which does not give such activity. CO_2ER over thin film electrode specifically forms CO(g) and Ethanol(l), 2 and 12 electron reduction products, and eliminates the possibility of unwanted HER as a side reaction in the CO_2 saturated $NaHCO_3$ electrolyte. We achieved significant product selectivity and faradaic efficiency, utilizing the very low potential for both CO and ethanol. Specific formation of only CO and ethanol makes the process efficient as the separation of gas and liquid is easy. Results based on density functional theory calculations suggest that CuO (111) and CuO (-111) surfaces promote CO_2 adsorption and subsequent formation of CO. However, a direct CO-dimerization is observed only on the CuO (111) surface that facilitates the formation of ethanol as the C2 product. This comparative study of bulk and thin-film opens new insight and highlights the importance of catalyst fabrication for the specific product formation utilizing significantly less energy.

1. Introduction

The depletion of fossil fuels leads to the production of massive volumes of carbon dioxide (CO_2), which contributes significantly to climate change [1,2]. Hence, the conversion of CO_2 to valuable chemicals in the earth's atmosphere is of great significance [3] and is critical for the alleviation of global warming [4–7]. CO_2 is a well-known stable molecule, which requires high energy [8,9] for the conversion to the valuable products [10]. Literature suggests a tremendous amount of research on the CO_2 conversion by thermochemical [11,12], chemical reforming [13], biochemical [14,15], mineralization [16], electrocatalytic [17], and/or photo electrocatalytic routes [18,19]. Among these routes, electrocatalytic and/or photo electrocatalytic routes are the most promising and appealing approaches because of their advantages like the economically viable catalyst [20–22], feasible operating conditions (low temperature, pressure), controllable reaction rates, and good product selectivity. To obtain a specific product, catalyst selection and design also play a decisive role in CO_2ER [13,23–25]. Therefore, numerous heterogeneous catalyst formulations in the form of powder and thin films have been researched to enhance the CO_2 electrocatalytic reduction activity. Early experimental evidence dates back to the 1950s when Teeter and Rysselberghe utilized mercury electrode as a cathode to reduce CO_2 [26,27]. Later, Yoshio Hori and co-workers [28,29] studied various materials thoroughly and quantified both gaseous and liquid products. They concluded copper is the most active catalyst for the formation of useful hydrocarbons. Subsequent studies on copper electrode [30–32], Oxide derived Copper [33,34], Cu-Ag alloys [35,36], Cu-Pd alloy [37,38], $Cu_2Cd/Cd/Cu$ bimetallic catalyst, binary copper selenide [39] have been carried out in the literature. Similarly, transition metal oxides, RuO_2-based electrode [40], and mixed oxides [41] have been used with good activity towards CO_2ER. To enhance efficiency of electroreduction, large surface area plays a vital role which could be achieved by fabricating the electrode in the form of thin film. Thin films lead to advantageously improvement in product efficiency

* Corresponding author.
E-mail address: ssharma@iitgn.ac.in (S. Sharma).
[1] Equal contribution.
[2] orcid.org/0000-0002-5217-9941
[3] https://orcid.org/0000-0003-3029-8840

https://doi.org/10.1016/j.electacta.2022.141791
Received 13 November 2022; Accepted 27 December 2022
Available online 30 December 2022

because of accessible high active-site and high electric conductivity [42], facile chemical adsorption of reactant gas on the surface of electrocatalyst, product rearrangement over surface followed by desorption from electrode surface [43].

Carbon dioxide reduction to various hydrocarbons and alcohols such as methanol and ethanol can produce a valuable feedstock for chemical industries and fuels for our energy necessities [44]. Among the various products which CO_2ER offers, ethanol is an interesting and useful product for comprehensive utilization, including fuel cell [45]. Nevertheless, its formation is not easy as it is a kinetically slow 12 e^- process [46]. So, there is a requirement of efficient electrocatalyst which should be capable of lowering the electroreduction overpotentials for ethanol synthesis and in cognizance of this, an important goal is to tune the Cu based catalysts. In all the studies that exist in the literature, transformations to multi-electron products starts only at high potential, where the hydrogen evolution reaction (HER) becomes competitive, declining the efficiency of CO_2ER. Efficient catalysts must slow down the HER and be selective to the specific product(s) [47–49].

Several catalyst synthesis/fabrication routes have been utilized in literature, viz. chemical reduction [50–53], Solution Combustion [54], Magneton sputtering [55], Sol-gel method [56–60], Electrodeposition [61–64], and Chemical bath deposition [65]. The majority of the literature work is based on the creation of an oxide layer on the Cu foil or substrate after annealing in the air [66,67], electron beam evaporation [68] and thermal evaporation [69]. Most of the synthesis routes require the presence of stabilizers, ligands, and binders for the synthesis and stability of the catalyst, making the synthesis process tedious, time-consuming, and non-economical.

Thus, to circumvent the drawback, this work is designed to synthesize copper oxide in the form of semi-transparent thin film by the sol-gel method on a conductive F-doped SnO_2 coated glass (FTO) substrate. The method brings in some novel advantages associate with the thin film electrode. The method of preparation is simple and scalable and does not require any additional stabilizer, binder, etc. The unique advantage of CuO thin film over bulk CuO for CO_2 electroreduction is demonstrated by the comparative studies of the two systems. Thin film electrode shows remarkable differences in faradaic efficiency and overvoltage in comparison to the bulk counterpart. The facet effect of copper crystal promotes CO adsorption and C—C coupling process and it is the most critical step for generating multi-carbon products [21,68,69]. However, to the best of author's knowledge, extensive research on crystal facets on bulk CuO thin film has not been carried out in the literature and this is the most novel feature of our studies

2. Experimental section

2.1. Precursors and materials

The chemicals used were $CuNO_3{\cdot}3H_2O$, Citric acid monohydrate, and Sodium bicarbonate ($NaHCO_3$). The films were synthesized on F-doped SnO_2 coated glass (FTO) substrates to integrate the working electrode. Ultra-pure deionized water (resistivity 18 MΩ cm) was taken the Merck Millipore water purification system to prepare electrolyte, cleaning electrodes, and electrochemical setup (Fig. 1). The pH values of the prepared 0.5 M $NaHCO_3$ electrolyte (pre-and post-electrocatalysis) solution were determined with a Thermo-scientific pH meter. The pH of the electrolyte decreases after CO_2 purging because CO_2 is an acidic gas.

The working thin film electrode was fabricated via the following

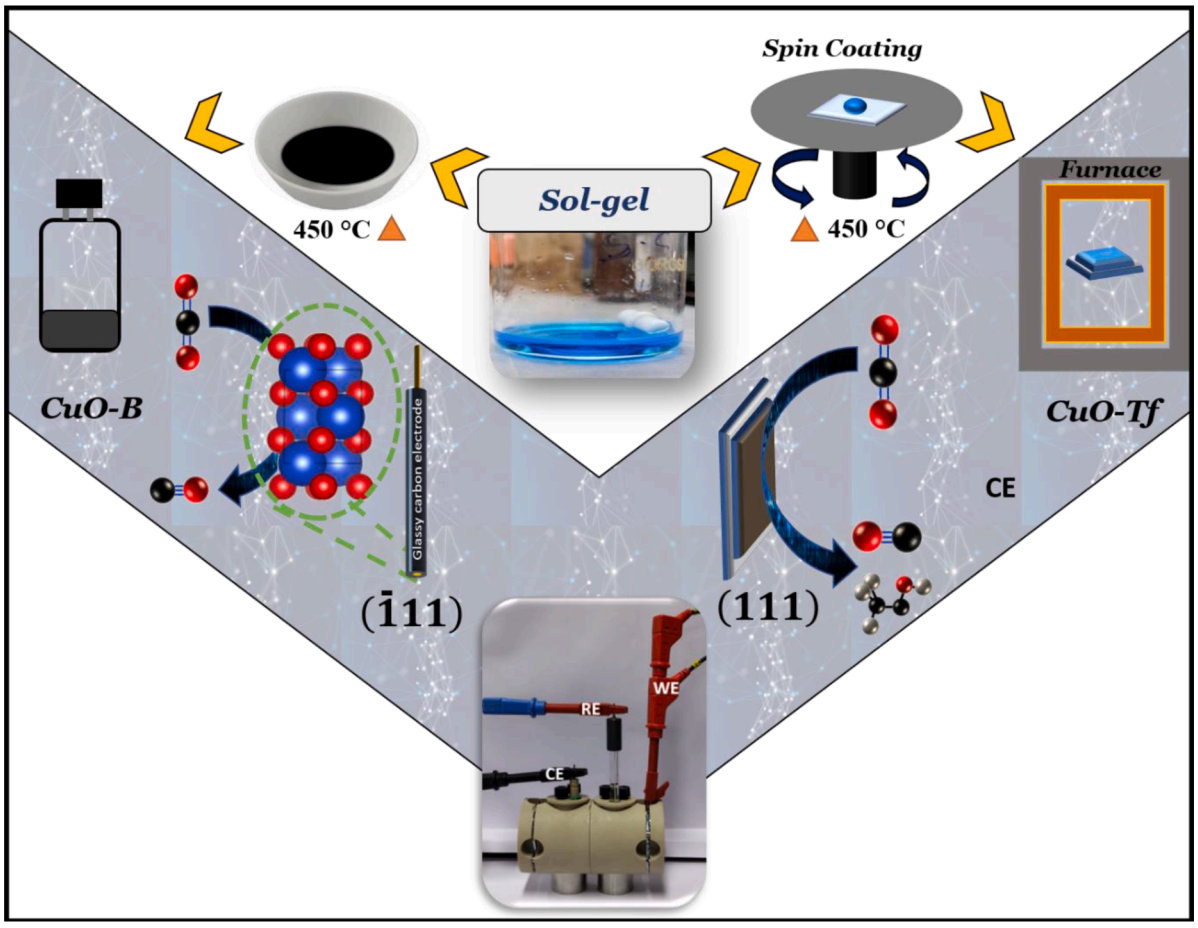

Fig. 1. A Schematic diagram of the synthesis protocol of CuO-tf and CuO-B by sol-gel method. Illustration of conventional electrochemical cell and their activity towards electrochemical reduction of CO_2.

method: The as purchased conductive FTO transparent electrodes were cleaned via sequential ultra-sonication by keeping it in a hot soap solution (1:3 Soap: DI water), hot DI water (80 °C), ethanol, and isopropyl alcohol each for 30 min, followed by drying at 75 °C in a hot air oven. As the initial synthesis step, Sol was prepared by adding $CuNO_3{\cdot}3H_2O$ solution dropwise to Citric acid (molar ratio 1:1.5). The prepared solution was stirred for 12 h at 40 °C on a magnetic stirrer and then kept for 48 h for ageing. Afterwards, the sol-gel batch was split into two parts (a) the prepared sol was spin-coated over FTO substrate by optimizing and controlling the deposition parameter (b) the remaining sol was kept in a muffle furnace in an alumina crucible for 20 min to prepare bulk powder material. In the second stage of synthesis, the spin-coated film and the synthesized powder were annealed in air at a higher temperature (450 °C) for 4 h in the Nebertherm Furnace with a heating rate of 5 °C/minute. We designate the fabricated thin film of CuO over FTO and bulk CuO as CuO-Tf and CuO-B, respectively.

2.2. Material characterization

The thickness and morphology of the synthesized thin films and bulk were analyzed by a JEOL (JSM-7900F) scanning electron microscope (SEM). An energy-dispersive X-ray spectrometer (EDS) instrument attached to the SEM, with AZtec (Oxford Instruments) software, was used for determination of film composition. Atomic Force Microscopy (Nano Scope Multimode 8.0, Bruker) was used to measure the surface profile and calculate the Roughness value of the sample. The tip used was SCANASYST-AIR in peak force tapping mode.

X-ray diffraction (XRD) was used to identify the crystallinity, phase constitution and crystal structure of the synthesized catalyst. A Rigaku Multipurpose X-ray diffractometer (Smartlab 9KW) with a Cu X-ray tube source (λ Kα = 1.54 Å) was used for Grazing incident angle X-ray diffraction (GIXRD) measurements. The XRD was operated at a working current and voltage of 100 mA and 45 kV, respectively. Continuous scans were performed from 10° to 90° (2θ mode, degree) using PB (parallel beam) optics at a scan rate of 4°/min (0.04° step size) with the incident angle held at 1° to analyze the samples of CuO-Tf. The CuO-B catalyst was characterized by using a Bruker D8 Discover diffractometer. Moreover, to understand the crystalline properties of thin film high resolution Transmission Electron Microscopic (HR-TEM) images were acquired at an accelerating voltage of 200 kV by using Thermo Titan Themis 300 kV. The sample was prepared over copper grid (300 mesh) by drop casting, which was allowed to dry for 30 min followed by UV ozone treatment for 10 min. Furthermore, to understand the chemical composition of the surface X-ray photoelectron spectroscopy (XPS) analysis of CuO thin film before and after electroreduction were carried out using Thermo scientific (NEXSA surface analysis system) with a micro-focused X-ray (400um, 72 W, 12,000 V) monochromatic Al-Kα source (hν = 1486.6 eV), a hemispherical analyzer, and a 128-channel plate detector. HRTEM images were recorded at PE for survey scan 200 eV and core scan 50 eV. Deconvolution of the recorded spectra was done by using linear function background in CASA software.

2.3. Electrochemical measurement

An electrochemical setup (supplier: Redox, Sweden) was used for thin-film electrocatalysis, in which a fixed area of 1 cm^2 was exposed during the reaction for the experiment. A fresh thin-film catalyst as a working electrode was used for potential dependent experiments to prevent the effect of degradation of catalyst layer on the distribution of product and for the precise calculation of gaseous analysis. Also, a custom electrochemical three-neck cell was constructed to check the electrocatalytic activity of bulk material. Both the electrochemical cells were divided and airtight to ensure all produced gasses were detected during the experiment. 0.5 M $NaHCO_3$ was used as electrolyte (25 ml electrolyte utilised for each experiment) in the CO_2ER experiments. At the beginning of each experiment, the electrochemical cell was purged using Alicat mass flow controller (MFC) at 10 SCCM with N_2 gas for 30 min to ensure the removal of dissolved oxygen and for inert atmosphere.

Similarly, CO_2 purging for 30 min before the electroreduction process is carried out to ensure saturation. After performing experiment of CO_2ER, the formed gaseous products were syringed out (using a high precision airtight syringe) then identified and quantified using Gas Chromatography (GC; Dhruva CIC Baroda (for gas detection) and Agilent 7890B Gas Chromatograph (for liquid detection). Nitrogen and Argon was used as a carrier gas for gas and liquid analysis respectively. A Thermal Conductivity Detector (TCD) and Flame Ionization Detector (FID) coupled with methaniser was used to quantify the generated gaseous and liquid products during the electroreduction process. The column used was the Agilent J&W Capillary column for liquid product analysis. Quantitative analysis of the product (number of moles of gas and liquid produced) by Calibration plot was carried out to corroborate the hypothesis of CO and Ethanol production (Figure S6).

2.4. CO_2 electroreduction procedure and product analysis

The CO_2ER experiments were performed using a AUTOLABPGSTAT302 N potentiostat with a working electrode (thin film cathode and glassy carbon electrode) and a counter platinum electrode, and Ag/AgCl reference electrode formed the three-electrode setup.

CO_2 Electroreduction activity was tested by running a Cyclic voltammetry (CV) at a 10 mV/s scan rate in the wide potential range from 0.4 V to −0.6 V and −0.8 V vs Ag/AgCl to characterize the electrochemical response. CVs in the fixed potential window (0.0 V to −0.6 V and −0.8 V), and then the CO_2ER at a fixed potential. The CO_2ER experiment was carried out at room temperature and at several different potentials to get a measurable volume of gaseous products for quantification using gas chromatography. The Faradaic Efficiency (FE) was calculated based on the required number of electrons to form one molecule of product from CO_2 during the electroreduction process.

3. Theoretical methods

Electronic structure calculations were based on density functional theory (DFT) and were performed with the Quickstep [70] module provided by the CP2K program [71]. Exchange-correlation potentials were treated within the generalized gradient approximation (GGA) employing the Perdew-Burke-Ernzerhof (PBE) functional [72]. The GGA formalism has been demonstrated to yield reasonably accurate results for studying CO_2 adsorption [73] and electrochemical CO_2 reduction [74] on metal-oxide surfaces. A double-ζ valence plus polarization (DZVP) basis set, optimized according to the Mol-Opt method [75], was adopted to expand the wavefunctions. The energy cutoff was set to 400 Ry for the auxiliary plane wave expansion of the charge density. Valence electrons were modelled explicitly, whereas core electrons have been treated with norm-conserving Goedecker-Teter-Hutter (GTH) potentials [76] with 1, 4, 6, and 11 valence electrons for H, C, O, and Cu, respectively. Integration of the Brillouin zone was performed with a reciprocal space mesh consisting of only the gamma point. The DFT-D3 van der Waals corrections by Grimme [77] were applied to take into account the long-range dispersion forces, which is essential for the accurate description of the interaction between the adsorbate and CuO surfaces. All calculations were performed with periodic boundary conditions.

In this study, steps involved in the CO_2ER process have been investigated on the CuO (111) and CuO (−111) surfaces using standard DFT calculations. For the CuO (111) and CuO (−111) surfaces, we have used 5 × 2 and 4 × 3 unit cells containing 60 and 72 Cu atoms, respectively. In both cases, the slab consists of three layers, of which the top layer was allowed to relax while the bottom layers were fixed to simulate the bulk properties. Adsorption of CO_2 and other intermediate species was simulated on one exposed surface. The (111) and (−111) surfaces were realized by introducing a vacuum of 15 Å along the [111] and [−111]

directions to avoid interaction with the periodic images of the slab. The atoms of the adsorbate and the topmost layer of the slab were allowed to relax unconstrainedly until the residual forces on all atoms reached 4.5 $\times 10^{-4}$ a.u.

4. Result & discussion

4.1. Characterization

As synthesized CuO-Tf catalyst was analyzed for crystal structure identification by Grazing Incident angle X-ray Diffraction (GIXRD). The crystallinity of prepared electrocatalysts is confirmed by intense and sharp peaks in XRD pattern (Fig. 2a). The XRD pattern show (110), ($\bar{1}$11), (111), (200) planes at 32.50, 35.53, 38.73, 38.94 (2 theta) peaks for both CuO-B and CuO-Tf. The magnified view of the XRD peak associated with the most intense peak of CuO-Tf (incident angle 0.4°) is represented in Figure S2 (b), where only the CuO peak can be observed where the preferential orientation of the (111) plane is visible clearly. XRD diffraction pattern of the CuO-Tf and CuO-B reveals that the catalyst crystallizes in the monoclinic crystal structure (00–041–0254) with 9.2 nm and 22.2 nm average crystallite size obtained by Scherrer's equation (expressions for calculations are shown in supporting information in Section 2.2). The ratio of the most intense peak $I_{(\bar{1}11)}$: $I_{(111)}$ for CuO-Tf is (0.877: 1) and CuO-B is (1.038: 1). The data reveals that (111) is preferentially oriented in the case of CuO-Tf while CuO-B is a regular polycrystalline material. It is well known that electrocatalytic activity is a strong function of catalytic activity, and different facets can lead to different product distribution. Therefore, it is expected that both CuO-Tf and CuO-B will show different catalytic activity. Moreover, the peak broadening feature of CuO-Tf is distinguishable from CuO-B (Fig. 2a) pointing out the small-sized CuO crystallites on the film electrode.

The surface micrograph (Fig. 2d) and cross-sectional (Fig. 2e) of CuO-Tf reveal that the coating of film on the FTO substrate is quite homogeneous throughout, with a thickness of 425 nm. CuO-B analysis by SEM (Fig. 2b) reveals an almost agglomerated spherical type particle with an average diameter of ~73 nm (Fig. 2c)

The roughness and surface morphology of prepared CuO thin film on the FTO substrate was investigated using AFM in peak force tapping mode. Fig. 2d shows the AFM image of CuO thin film in 3D mode. The surface topographical image shows a homogeneous surface with closely packed grains and an average roughness value of 8.41 nm. Close packing of grains is good for conductivity in the thin films and turn, for good electrochemical activity.

To better understand the crystalline properties and morphology of the CuO in thin films, we performed high-resolution transmission electron microscopy (HRTEM). The HRTEM image exhibited a lattice fringe spaced by 2.32 angstrom, corresponding to the (111) plane of CuO (Fig. 3b). Thus, the thin films are crystalline and have prominent (111)

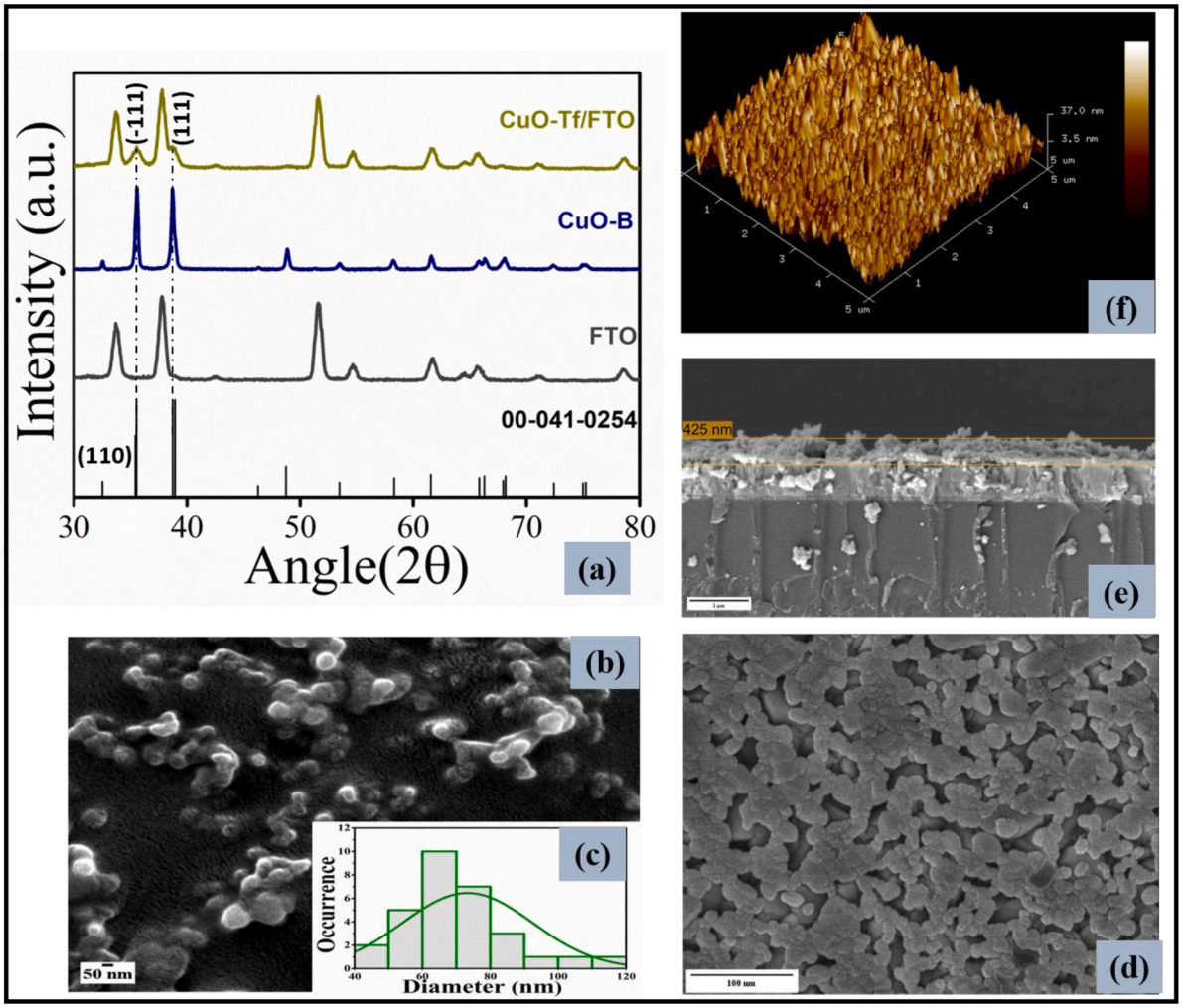

Fig. 2. (a) X-ray diffractograms of FTO, CuO bulk and CuO thin film, FESEM image of (b) CuO-B and (d) CuO-Tf, (c) Histogram distribution of the particle size of CuO-B with an average diameter of 73.29 nm, (e) Cross-sectional image of as-prepared thin film, (f) 3D AFM image of the as-synthesized CuO thin films deposited at 450 °C.

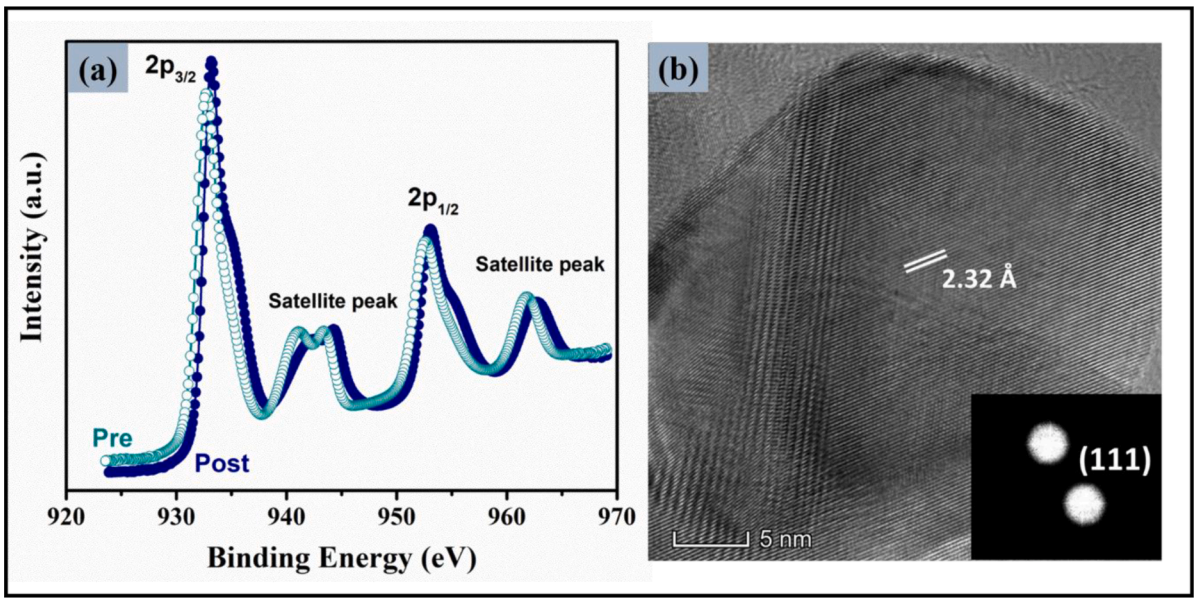

Fig. 3. (a) The compiled high-resolution Cu XPS curve for pre- and post-reaction over CuO thin film. (b) HRTEM images of the scraped CuO thin film and inset shows the masked region of diffraction spots for inverse FFT derivation of respective figures.

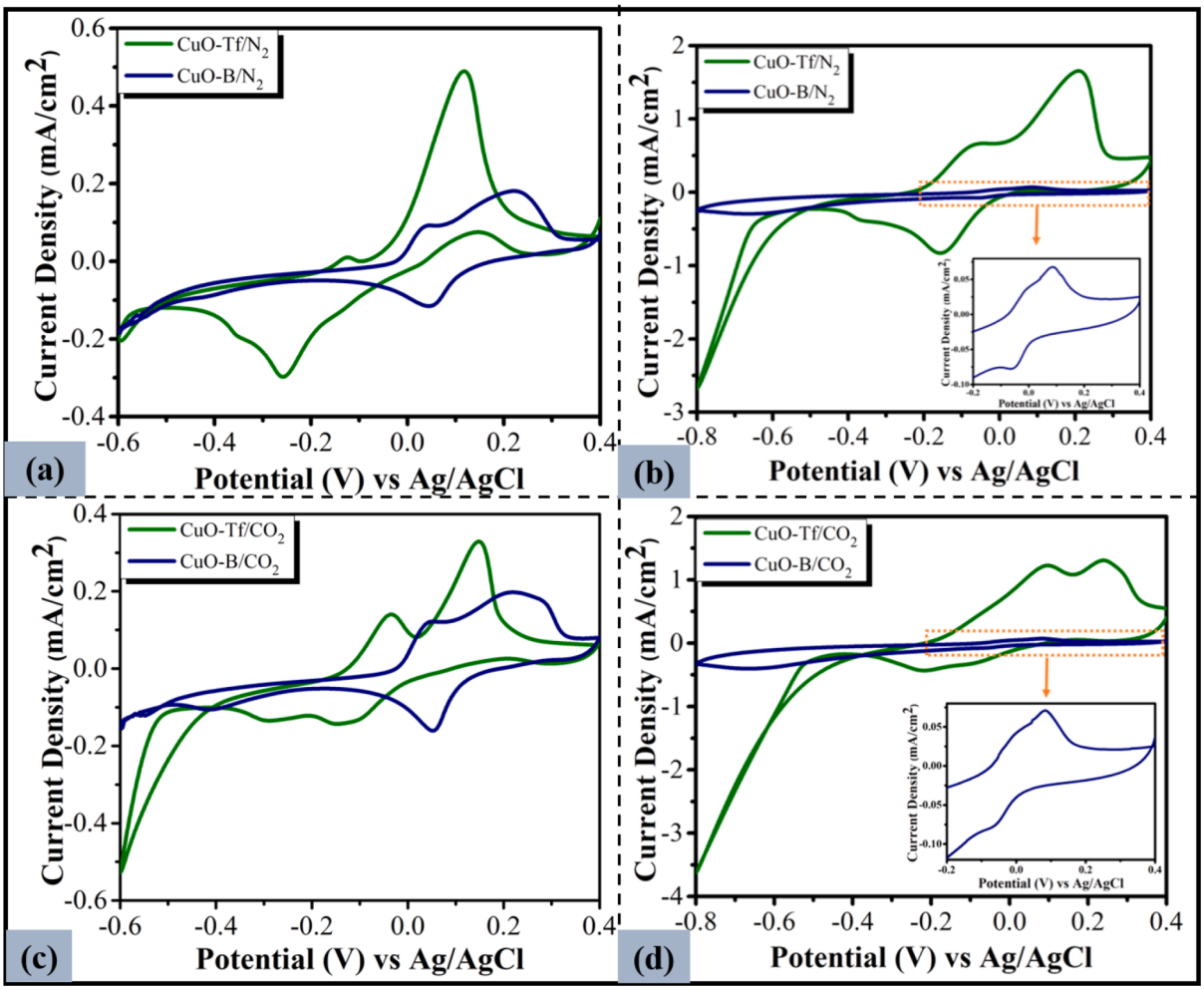

Fig. 4. Cyclic Voltammetry response of CuO-Tf (Olive trace) and CuO-B (Navy trace) in Nitrogen purged solution (a,b) and CO_2 saturated solution (c,d) at a potential range of 0.4 V to −0.6 V and 0.4 V to −0.8 V in an electrocatalytic cell containing 0.5 M $NaHCO_3$ solution at a scan rate of 10 mV/*sec*. Inset images of (b) and (c) are a magnified view of CuO-B in a potential range from 0.4 V to −0.2 V.

crystal facet. Particles are agglomerated with size of 20–30 nm, bigger than estimated from the XRD.

To further understand the chemical composition of the surface, high-resolution XPS spectra of Cu 2p in CuO thin film are recorded before and after CO_2 electroreduction (Fig. 3a). Both the spectra are nearly identical to each other explaining that the surface is stable after the electroreduction experiment. Further, the deconvoluted high-resolution XPS (Figure S5) of Cu 2p with doublets, Cu $2p_{3/2}$ and Cu $2p_{1/2}$ at 934.1 eV and 953.8 along with the satellite peaks at 943.6 eV, 941.1 eV and 961.8 eV are an indicative of Cu^{2+} oxidation state in fresh catalyst. A minor contribution from Cu^{1+} is also present along with Cu $2p_{3/2}$ and Cu $2p_{1/2}$ peaks at 932.6 eV and 952.4 eV. All the binding energy values, match well with the reported studies [78,79]. Thus, the major oxidation state on the CuO-Tf surface is Cu^{2+}. Even after the reaction, the Cu^{2+} peaks appear at nearly the same BE values. The surface composition before the reaction is 66% for Cu^{2+} and 34% from Cu^{+} which changes to 76% and 24% for Cu^{2+} and Cu^{1+} respectively. These parameters confirms that Cu^{2+} remains the major oxidation state under all the condition and this is the stable species on the surface.

4.2. Electrochemical studies

Cyclic Voltammetry (CV) studies of CuO thin film (CuO-Tf) and CuO bulk powder (CuO-B) is shown in Fig. 4, which were done to understand and compare the basic electrochemical and electrocatalytic properties of the synthesized catalysts. Wide potential ranges from 0.4 V to −0.6 V and 0.4 V to −0.8 V vs Ag/AgCl reference electrode were selected for the electrochemical studies. The working potential window is restricted to the mentioned range to discard the possibilities of Hydrogen Evolution Reaction (HER).

There are noticeable changes in terms of current density and peak potential in CuO-Tf and CuO-B, which can be observed in Fig. 4 (a,b). The peak shape in CuO-B is broad and poorly resolved in the range of 0.4 V to −0.6 V, unlike CuO-Tf, where the peaks are sharp and well resolved. Moreover, the anodic and cathodic peaks are shifted significantly in CuO-Tf compared to CuO-B. In terms of the possible chemical reactions, the CuO-Tf catalyst shows two anodic peaks, which correspond to the oxidation of Cu^0 to Cu_2O and CuO at −0.12 V and 0.11 V (vs Ag/AgCl). Also, two cathodic peaks at −0.25 V and −0.35 V (vs Ag/AgCl) correspond to the reduction of CuO to Cu_2O and Cu^0, respectively [49]. CuO-B shows two anodic peaks at 0.04 V and 0.22 V (vs Ag/AgCl) for Cu^0 to Cu_2O and CuO, and a cathodic peak at 0.041 V is the one-step reduction of CuO to Cu^0. The more exposed area and smaller crystallite size in CuO-Tf may result in intense and well-resolved peaks compared to the CuO-B. Cyclic voltammetry studies in the extended cathodic potential window, i.e., 0.4 V to −0.8 V (Fig. 4b), are also studied for CuO-Tf and CuO-B. Not much change is observed in CuO-B in terms of peak shape and peak current density (Fig. 4b inset). On the other hand, in CuO-Tf, the peak at −0.12 (Cu→Cu_2O) becomes significantly intense due to the enhanced reduction of metallic Cu. In addition, a steep current rise is also noticed at the onset of −0.5 V.

CV response after CO_2 saturation in the electrolyte shows only a minor increase in the current in the case of CuO-B at −0.6 V. Still; the current is significantly higher in the case of CuO-Tf (Fig. 4c).

Quantitively, the current increases from |0.2| mA/cm^2 to |0.5| mA/cm^2, i.e., 2.5 times at −0.6 V. Even in the broader potential range, −0.6 V and −0.8 V, CuO-B does not show much change, while CuO-Tf shows ~1.4 times enhancement in the current at −0.8 V (Fig. 4d). This proves that CuO-Tf has considerable CO_2 electroreduction activity. An enhancement in reduction current under CO_2 dissolution indicates an active catalytic behavior of CuO-Tf towards the electroreduction of CO_2 under varied potential ranges. The synthesized film is unstable at a higher applied potential (greater than −0.8 V) as the film rips off after the first cycle from the FTO surface. Hence, we restrict our potential window to −0.8 V only.

The electrocatalytic activity is also investigated in the potential ranges; of 0.0 to −0.6 V and 0.0 V to −0.8 V (Fig. 4) for both CuO-Tf and CuO-B. Similar to the previous data, CuO-B does not show a noticeable increase in the current before and after CO_2 saturation in both the potential ranges (data not shown). In contrast, CuO-Tf shows enhanced current densities under similar voltage ranges compared to FTO in both N_2 (Figure S1) and CO_2 saturated solutions (Fig. 4). In the presence of N_2, catalytic current in CuO-Tf increases by ten times at −0.6 V (Figure S1a) and 13 times at −0.8 V compared to bare FTO (Figure S1b). The reduction current further intensifies by ~1.4 times at −0.6 V (Fig. 4a) and ~1.6 times at −0.8 V (Fig. 4b) after CO_2 saturation. The onset voltage for CO_2 electroreduction is −0.4 V (vs Ag/AgCl)) for CuO-Tf, as evident from Fig. 4a and Fig. 4b.

In practical applications, product selectivity, faradaic efficiency and stability are the vital parameters of electrocatalysts. These are evaluated by performing a time dependent current density curve under steady state electrocatalysis for 30 min (chronoamperometry) at −0.6 V and −0.8 V in CO_2 saturated $NaHCO_3$ solution (Figure S2). Due to the complex mechanism of product formation, current density alone cannot provide conclusive evidence regarding the activity of the catalyst. Therefore, the product analysis is carried out using gas chromatography after the chronoamperometry experiment.

Selective production of gaseous CO and liquid ethanol happens exclusively at −0.6 V (vs Ag/AgCl) after the CO_2ER process, as shown in Fig. 5d. This voltage corresponds to −0.05 V vs reversible Hydrogen Electrode (RHE) after IR correction and considering a 10% error in the measurement. This voltage is close to the thermodynamic voltage for the conversion of CO_2 to CO. Notably, this voltage corresponds to an ultra-low overpotential (140 mV) for the ethanol formation from CO_2. These products' yield for CuO-Tf increases significantly when the potential increases to −0.8 V (vs Ag/AgCl) or −0.25 V (vs RHE). CuO-B does not form any product at −0.6 V, i.e., CO_2ER does not start at this potential for this catalyst. On shifting potential toward −0.8 V, CuO-B exclusively produces CO with a Faradaic efficiency of around 4.0 ± 0.47%, confirming the low activity of this catalyst. Faradaic Efficiencies for the two major products, namely CO and ethanol, are 13.1 ± 0.59% and 13.2 ± 0.47%, at −0.6 V and 23.5 ± 0.85% and 23.4 ± 1.01%, respectively, at −0.8 V over CuO-Tf. Almost equal distribution of product efficiency at both the voltages suggests that CO could be a reactive intermediate that is participating in the ethanol production as per the reaction [80],

$$CO + 8H^+ + 8e^- \rightarrow CH_3CH_2OH + H_2O,\ E^0 = 0.19\ V$$

The overvoltage for this reaction is 240 mV which is also quite low. Hydrogen production does not happen under the studied potential ranges for CuO-B and CuO-Tf, discarding the possibility of unwanted side reactions (HER) during CO_2ER.

To verify the possibility of CO intermediate for ethanol production, CO is dissolved in the electrolyte followed by the reduction at −0.6 V for 1800 s. This, however, does not yield any ethanol suggesting that externally dissolved CO is probably different from the intermediate generated during CO_2ER. High selectivity and a decent faradaic efficiency at such a low potential strengthen the fact that our fabrication methodology of preparing CuO-Tf electrocatalysts in the thin film has some unique active sites compared to CuO-B. This conclusion is backed up by the fact the CuO-Tf has a relatively more exposed (111) plane resulting in the unique activity and selectivity for CO and Ethanol. Thus, (111) facets in CuO-Tf are the active sites for CO_2ER to generate CO, an intermediate to convert ethanol. CO_2ER is also examined at lower potentials such as −0.55 V and −0.58 V, but no product was detected at this low applied potential, which confirms that product formation starts at −0.6 V only. It is worth noticing from Fig. 5c (detailed information is tabulated in Table S1) that very few studies utilize such low potentials to achieve significant ethanol production similar to the present study. It is also clear from Table S1 that synthesized CuO-Tf is unique (without noble metal) and has superior activity compared to other reported catalysts concerning liquid ethanol production. Also, to the best of our

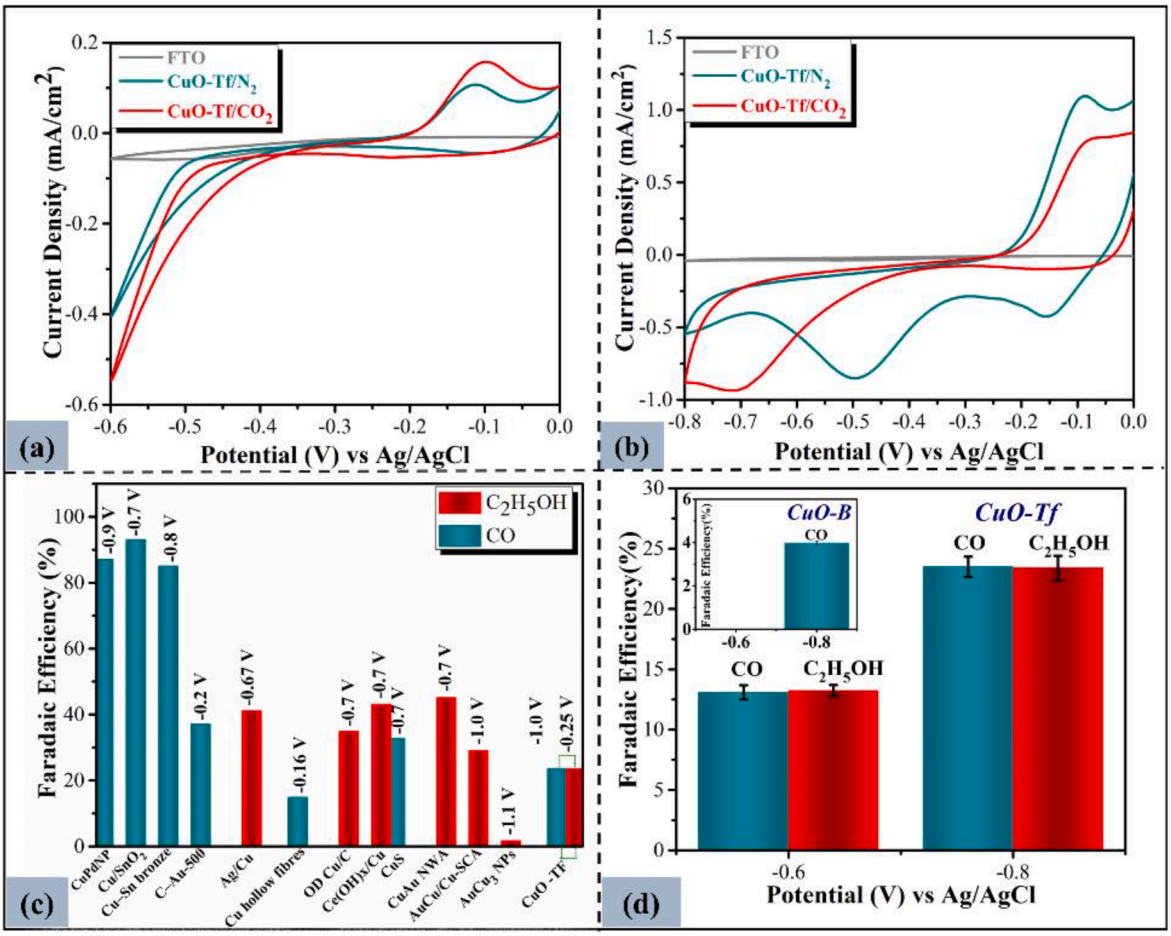

Fig. 5. Electroreduction Cyclic Voltammetry response of FTO (Gray trace) and CuO-Tf saturated with CO_2 gas (Dark Cyan trace) at a different applied voltage (a) −0.6 V and (b) −0.8 V in an electrocatalytic cell containing 0.5 M $NaHCO_3$ solution at a scan rate 10 mV/s. (c) Faradaic Efficiency for different electrocatalyst materials at certain applied potential (vs RHE) available in the literature for CO_2ER. (d) Faradaic Efficiency of the product obtained (CO and C_2H_5OH) after electroreduction for 1800 s is depicted in the bar diagram at potential of −0.6 V and −0.8 V (−0.05 V and −0.25 V vs RHE), and the inset represents the trend of CO_2ER products on the CuO-B. The standard deviations are shown as vertical lines.

knowledge, no study has achieved exclusive CO and ethanol production from CO_2 electroreduction at near thermodynamic potential, making CuO-Tf an excellent electrocatalyst. Exclusive production of gaseous CO and liquid ethanol is interesting because one can get pure CO and pure ethanol without undergoing a tedious separation process.

The CuO-Tf and CuO-B electrodes are subjected to post-XRD characterization, giving a unique perspective in assessing the active site. XRD is carried out after 30 min of chronoamperometry experiment in the CO_2 saturated electrolyte at −0.6 V. XRD pattern (Figure S2, b) of CuO-Tf reveals that complete transformation of CuO to Cu_2O occurs after the electrochemical analysis. Cu (+1) in Cu_2O is known to reduce CO_2 into ethanol [48,62,81]. However, it is not very selective and gives a range of products [82–86]. Nevertheless, CuO-Tf uniquely gives CO in the gas phase, and ethanol is a liquid phase with almost equal efficiency. At both −0.6 V and −0.8 V, both CO and ethanol form in equal amounts (Fig. 5d). Thus, there is a strong possibility that CO is possibly the precursor to ethanol formation as per the reaction [80];

$$CO + 8H^+ + 8e^- \rightarrow CH_3CH_2OH + H_2O,\ E^0 = 0.19\ V.$$

As per the moderation principle in catalysis, intermediate adsorption should be neither too weak nor too strong to achieve good product selectivity and Faradaic efficiency [87,88]. Literature suggests that CO has stronger adsorption over the Cu_2O surface in comparison to CuO [89] thus, it can sustain over the surface of Cu_2O long enough to get converted to ethanol. It is interesting to note that despite a surface phenomenon, the bulk structure of CuO-Tf is changing. It can be speculated that during the electroreduction, when surface CuO starts converting to Cu_2O, lattice oxygen is utilized which is replenished by the bulk lattice oxygen thus converting the overall bulk structure. Another reason could be the porosity in the film causing the bulk to change. In contrast, the XRD pattern of CuO-B indicates that CuO peaks are retained after CO_2 electroreduction confirming the stability of the bulk structure of the CuO-B catalyst. The weaker adsorption of CO over CuO does not let it stay over the surface hence it desorbs easily as a CO_2ER product without converting further.

4.3. Density functional theory calculations

DFT calculations for the CO_2ER to CO and CH_3CH_2OH on CuO (111), and CuO (−111) surfaces were performed to gain insights into the reaction mechanism and the role of crystal facets representing either CuO-Tf or CuO-B. The optimized structures of the key intermediates on the CuO (111) surface are displayed in Supplementary Figures S3 and S4. The consensus regarding the C—C coupling mechanism on copper and CuO surfaces is that adsorbed CO_2 is first reduced to form CO that subsequently undergoes dimerization to adsorbed OC*C*O, leading to the formation of various C_2 products [90–92] . Our DFT calculations demonstrated that CO_2 could be easily converted to adsorbed CO (*CO) via a *COOH intermediate on both CuO (111) and CuO (−111) surfaces. As in the next step, the formation of an O*C*CO intermediate from *CO on the CuO (111) surface requires 0.4 eV (Fig. 6), indicating that C—C coupling through *CO dimerization is quite facile. Our DFT calculations have shown that the formation of the CO dimer is most stable on square

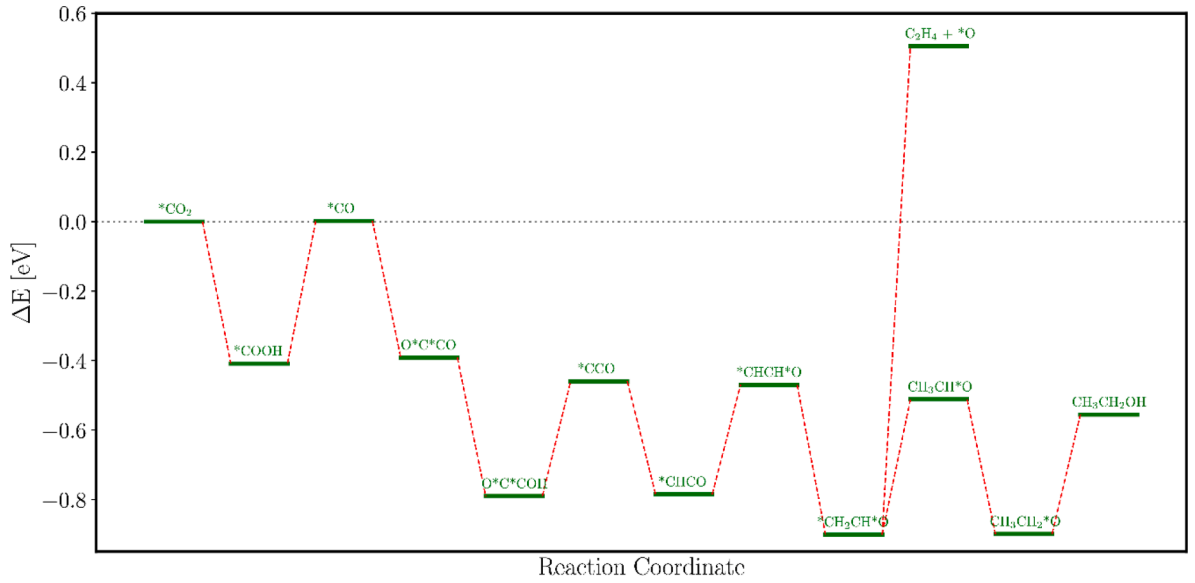

Fig. 6. A reaction energy diagram for the CO_2ER to CO and C_2H_5OH on CuO (111) facet via a direct *CO dimerization pathway.

arrangements of four surface atoms (Figure S3) on the CuO (111) surface. The barrier for dimer formation was found to be around 0.4 eV. The dimer intermediate further undergoes a proton-electron concerted reaction and forms another intermediate *CCO which subsequently leads to the formation of the CH_2CHO* intermediate. According to a report by Kortlever et al. [93], this species can either release a C_2H_4 or form another intermediate CH_3CHO*as a next step. The calculations have shown that the formation of CH_3CHO* species draws a lower energy barrier than the former (Fig. 6). Therefore, the reaction proceeds further to generate C_2H_5OH as another important C_2 product. The absence of any trace of C_2H_4 in the experimental measurements further substantiates our finding based on electronic structure calculations.

On the other hand, the formation of a dimer from the adsorbed CO (*CO) on the CuO (−111) surface was not observed in our simulations. The CO dimer species seemed to be unstable over the surface as the two monomer species (*CO) repel each other, as can be seen from Figure S4 in the Supplementary Information. We further studied the possibility of C—C coupling on different sites available on the CuO (−111) surface, however, there was no sign of the formation of a dimer intermediate. Indeed, this is an important observation since it correlates with the experimental measurements where CO was predominantly found at the higher applied voltage on the CuO-B. In short, the DFT calculations suggest that the reduction of CO_2 to *CO via *COOH, followed by the dimerization of *CO to O*C*CO, is the most favorable pathway for the formation of C_2H_5OH over the CuO-Tf. The adsorbed *CO thus acts as an intermediate step for the C—C coupling and at the same time results in the secondary product as CO (g) in the CO_2ER process.

5. Conclusion

Copper Oxide thin films are fabricated via the sol-gel spin coating method, which gives a highly active and selective CuO thin film (CuO-Tf) electrocatalyst for CO_2 electroreduction reaction. The optimized synthesis procedure is very facile and results in a relatively more exposed (111) crystal plane which is the reason for the formation of ethanol at near thermodynamic potential (140 mV overvoltage). Ethanol formation is a 12 e^- transfer reaction, and its formation at such ultra-low-voltage is not known in literature over any form of CuO. CO is also detected in the gas phase with almost equal faradaic efficiency. Almost equal distribution of product efficiency for CO and C_2H_5OH at different applied voltages indicates that CO could be a reactive intermediate during reaction participating in the ethanol production. There is no literature as of our knowledge where the fabrication of such a thin film has been reported and which shows the CO and ethanol selectivity as mentioned in our manuscript. Our investigation will pave a path for utilizing CuO thin film for conversion of greenhouse gas (CO_2) to CO and Ethanol. This technique could be promising to commercialize the process because of low-cost fabrication methodology, assembly, and facile separation of obtained products as CO is in gaseous form and ethanol in liquid form.

Declaration of Competing Interest

Sudhanshu Sharma reports financial support was provided by India Ministry of Science & Technology Department of Science and Technology.

Data Availability

Data will be made available on request.

Acknowledgements

SS acknowledges DST (DST/P0117/1092) and MHRD (STARS/APR2019/CS/215/FS) projects for the funding and fellowship. SD is thankful for the support from IITGN for the fellowship. JN acknowledges CSIR for fellowship. SD, JN, and VK acknowledge IITGN for the CIF facility. AM acknowledges IITGN and CDAC [PARAM Siddhi-AI System] for the computational facility.

Supplementary materials

Supplementary material associated with this article can be found, in the online version, at doi:10.1016/j.electacta.2022.141791.

Reference

[1] P. Friedlingstein, M.W. Jones, M. O'Sullivan, R.M. Andrew, D.C.E. Bakker, J. Hauck, C. Le Quéré, G.P. Peters, W. Peters, J. Pongratz, S. Sitch, J.G. Canadell, P. Ciais, R.B. Jackson, S.R. Alin, P. Anthoni, N.R. Bates, M. Becker, N. Bellouin, L. Bopp, T.T.T. Chau, F. Chevallier, L.P. Chini, M. Cronin, K.I. Currie, B. Decharme, L.M. Djeutchouang, X. Dou, W. Evans, R.A. Feely, L. Feng, T. Gasser, D. Gilfillan, T. Gkritzalis, G. Grassi, L. Gregor, N. Gruber, Ö. Gürses, I. Harris, R.A. Houghton, G.C. Hurtt, Y. Iida, T. Ilyina, I.T. Luijkx, A. Jain, S.D. Jones, E. Kato, D. Kennedy, K. Klein Goldewijk, J. Knauer, J.I. Korsbakken, A. Körtzinger, P. Landschützer, S.

K. Lauvset, N. Lefèvre, S. Lienert, J. Liu, G. Marland, P.C. McGuire, J.R. Melton, D. R. Munro, J.E.M.S. Nabel, S.-I. Nakaoka, Y. Niwa, T. Ono, D. Pierrot, B. Poulter, G. Rehder, L. Resplandy, E. Robertson, C. Rödenbeck, T.M. Rosan, J. Schwinger, C. Schwingshackl, R. Séférian, A.J. Sutton, C. Sweeney, T. Tanhua, P.P. Tans, H. Tian, B. Tilbrook, F. Tubiello, G.R. van der Werf, N. Vuichard, C. Wada, R. Wanninkhof, A.J. Watson, D. Willis, A.J. Wiltshire, W. Yuan, C. Yue, X. Yue, S. Zaehle, J. Zeng, Global carbon budget 2021, Earth System Science Data 14 (2022) 1917–2005, https://doi.org/10.5194/essd-14-1917-2022.

[2] G. Wang, J. Chen, Y. Ding, P. Cai, L. Yi, Y. Li, C. Tu, Y. Hou, Z. Wen, L. Dai, Electrocatalysis for CO 2 conversion: from fundamentals to value-added products, Chem. Soc. Rev. (2021), https://doi.org/10.1039/D0CS00071J.

[3] P. De Luna, C. Hahn, D. Higgins, S.A. Jaffer, T.F. Jaramillo, E.H. Sargent, What would it take for renewably powered electrosynthesis to displace petrochemical processes? Science 364 (2019) eaav3506, https://doi.org/10.1126/science.aav3506.

[4] C. Le Quéré, J.I. Korsbakken, C. Wilson, J. Tosun, R. Andrew, R.J. Andres, J. G. Canadell, A. Jordan, G.P. Peters, D.P. van Vuuren, Drivers of declining CO2 emissions in 18 developed economies, Nat. Clim. Chang. 9 (2019) 213–217, https://doi.org/10.1038/s41558-019-0419-7.

[5] J. Rogelj, G. Luderer, R.C. Pietzcker, E. Kriegler, M. Schaeffer, V. Krey, K. Riahi, Energy system transformations for limiting end-of-century warming to below 1.5°C, Nature Clim Change 5 (2015) 519–527, https://doi.org/10.1038/nclimate2572.

[6] T.A. Jacobson, J.S. Kler, M.T. Hernke, R.K. Braun, K.C. Meyer, W.E. Funk, Direct human health risks of increased atmospheric carbon dioxide, Nature Sustain. 2 (2019) 691–701, https://doi.org/10.1038/s41893-019-0323-1.

[7] L. Lu, J.S. Guest, C.A. Peters, X. Zhu, G.H. Rau, Z.J. Ren, Wastewater treatment for carbon capture and utilization, Nat Sustain. 1 (2018) 750–758, https://doi.org/10.1038/s41893-018-0187-9.

[8] S. Subramanian, Y. Song, D. Kim, C.T. Yavuz, Redox and nonredox CO2 utilization: dry reforming of methane and catalytic cyclic carbonate formation, ACS Energy Lett. 5 (2020) 1689–1700, https://doi.org/10.1021/acsenergylett.0c00406.

[9] B. deB Darwent, National Standard Reference Data System (U.S.), Bond Dissociation Energies in Simple Molecules, U.S. Dept. of Commerce, National Bureau of Standards, Washington, D.C., 1970. https://purl.fdlp.gov/GPO/LPS116847 (accessed October 9, 2021).

[10] M.D. Garba, M. Usman, S. Khan, F. Shehzad, A. Galadima, M.F. Ehsan, A. S. Ghanem, M. Humayun, CO2 towards fuels: a review of catalytic conversion of carbon dioxide to hydrocarbons, J. Environ. Chem. Eng. 9 (2021), 104756, https://doi.org/10.1016/j.jece.2020.104756.

[11] S. Roy, A. Cherevotan, S.C. Peter, Thermochemical CO2 hydrogenation to single carbon products: scientific and technological challenges, ACS Energy Lett. 3 (2018) 1938–1966, https://doi.org/10.1021/acsenergylett.8b00740.

[12] S. Bhattacharyya, S. Roy, P.M. Ajayan, An Overview of Catalytic CO2 Conversion, in: Energy Transition: Climate Action and Circularity, American Chemical Society, 2022, pp. 411–468, https://doi.org/10.1021/bk-2022-1412.ch009.

[13] L. Wang, W. Chen, D. Zhang, Y. Du, R. Amal, S. Qiao, J. Wu, Z. Yin, Surface strategies for catalytic CO2 reduction: from two-dimensional materials to nanoclusters to single atoms, Chem. Soc. Rev. 48 (2019) 5310–5349, https://doi.org/10.1039/C9CS00163H.

[14] S. Saqib, A. Mukhtar, S. Ullah, M. Sagir, M.B. Tahir, R. Amen, M. Babar, A.G. Al-Sehemi, M.A. Assiri, M. Ibrahim, Biological methods for carbon dioxide conversion and utilization, in: A.Khan Inamuddin (Ed.), Sustainable Bioconversion of Waste to Value Added Products, Springer International Publishing, Cham, 2021, pp. 165–177, https://doi.org/10.1007/978-3-030-61837-7_10.

[15] P.R. Yaashikaa, P. Senthil Kumar, S.J. Varjani, A. Saravanan, A review on photochemical, biochemical and electrochemical transformation of CO2 into value-added products, J. CO2 Utiliz. 33 (2019) 131–147, https://doi.org/10.1016/j.jcou.2019.05.017.

[16] Q. Wang, Y. Lei, D. Wang, Y. Li, Defect engineering in earth-abundant electrocatalysts for CO2 and N2 reduction, Energy Environ. Sci. 12 (2019) 1730–1750, https://doi.org/10.1039/C8EE03781G.

[17] Y. Zhao, G.I.N. Waterhouse, G. Chen, X. Xiong, L.-.Z. Wu, C.-.H. Tung, T. Zhang, Two-dimensional-related catalytic materials for solar-driven conversion of COx into valuable chemical feedstocks, Chem. Soc. Rev. 48 (2019) 1972–2010, https://doi.org/10.1039/C8CS00607E.

[18] V. Kumaravel, J. Bartlett, S.C. Pillai, Photoelectrochemical conversion of carbon dioxide (CO2) into fuels and value-added products, ACS Energy Lett. 5 (2020) 486–519, https://doi.org/10.1021/acsenergylett.9b02585.

[19] B. Tang, F.-.X. Xiao, An overview of solar-driven photoelectrochemical CO2 conversion to chemical fuels, ACS Catal. 12 (2022) 9023–9057, https://doi.org/10.1021/acscatal.2c01667.

[20] S.N. Talapaneni, G. Singh, I.Y. Kim, K. AlBahily, A.H. Al-Muhtaseb, A.S. Karakoti, E. Tavakkoli, A. Vinu, Nanostructured carbon nitrides for CO2 capture and conversion, Adv. Mater. 32 (2020), 1904635, https://doi.org/10.1002/adma.201904635.

[21] B. Liu, C. Cai, B. Yang, K. Chen, Y. Long, Q. Wang, S. Wang, G. Chen, H. Li, J. Hu, J. Fu, M. Liu, Intermediate enrichment effect of porous Cu catalyst for CO2 electroreduction to C2 fuels, Electrochim. Acta 388 (2021), 138552, https://doi.org/10.1016/j.electacta.2021.138552.

[22] D. Wakerley, S. Lamaison, J. Wicks, A. Clemens, J. Feaster, D. Corral, S.A. Jaffer, A. Sarkar, M. Fontecave, E.B. Duoss, S. Baker, E.H. Sargent, T.F. Jaramillo, C. Hahn, Gas diffusion electrodes, reactor designs and key metrics of low-temperature CO2 electrolysers, Nat. Energy 7 (2022) 130–143, https://doi.org/10.1038/s41560-021-00973-9.

[23] S. Zhu, M. Shao, Surface structure and composition effects on electrochemical reduction of carbon dioxide, J. Solid State Electrochem. 4 (2016) 861–873, https://doi.org/10.1007/s10008-015-2884-x.

[24] Y. Wang, P. Han, X. Lv, L. Zhang, G. Zheng, Defect and interface engineering for aqueous electrocatalytic CO2 reduction, Joule 2 (2018) 2551–2582, https://doi.org/10.1016/j.joule.2018.09.021.

[25] C. Zhu, Z. Zhang, L. Zhong, C.-.S. Hsu, X. Xu, Y. Li, S. Zhao, S. Chen, J. Yu, S. Chen, M. Wu, P. Gao, S. Li, H.M. Chen, K. Liu, L. Zhang, Product-specific active site motifs of Cu for electrochemical CO2 reduction, Chem. 7 (2021) 406–420, https://doi.org/10.1016/j.chempr.2020.10.018.

[26] P. van Rysselberghe, G.J. Alkire, J.M. McGee, Polarographic reduction of carbon dioxide. III. Description and interpretation of the waves1, J. Am. Chem. Soc. 68 (1946) 2050–2055, https://doi.org/10.1021/ja01214a053.

[27] T.E. Teeter, P.V. Rysselberghe, Reduction of carbon dioxide on mercury cathodes, J. Chem. Phys. 22 (2004) 759, https://doi.org/10.1063/1.1740178.

[28] Y. Hori, K. Kikuchi, S. Suzuki, Production of co and ch4 in electrochemical reduction of co2 at metal electrodes in aqueous hydrogencarbonate solution, Chem. Lett. 14 (1985) 1695–1698, https://doi.org/10.1246/cl.1985.1695.

[29] 1985 Y. Hori PRODUCTION OF CO AND CH4.pdf, (n.d.).

[30] Y. Hori, K. Kikuchi, A. Murata, S. Suzuki, Production of methane and ethylene in electrochemical reduction of carbon dioxide at copper electrode in aqueous hydrogencarbonate solution, Chem. Lett. 15 (1986) 897–898, https://doi.org/10.1246/cl.1986.897.

[31] Y. Hori, A. Murata, R. Takahashi, S. Suzuki, Enhanced formation of ethylene and alcohols at ambient temperature and pressure in electrochemical reduction of carbon dioxide at a copper electrode, J. Chem. Soc., Chem. Commun. (1988) 17–19, https://doi.org/10.1039/C39880000017.

[32] S. Min, X. Yang, A.-.Y. Lu, C.-.C. Tseng, M.N. Hedhili, L.-.J. Li, K.-.W. Huang, Low overpotential and high current CO2 reduction with surface reconstructed Cu foam electrodes, Nano Energy 27 (2016) 121–129, https://doi.org/10.1016/j.nanoen.2016.06.043.

[33] M. Ma, K. Djanashvili, W.A. Smith, Selective electrochemical reduction of CO2 to CO on CuO-derived Cu nanowires, Phys. Chem. Chem. Phys. 17 (2015) 20861–20867, https://doi.org/10.1039/C5CP03559G.

[34] Y. Lum, B. Yue, P. Lobaccaro, A.T. Bell, J.W. Ager, Optimizing C–C coupling on oxide-derived copper catalysts for electrochemical CO2 reduction, J. Phys. Chem. C. 121 (2017) 14191–14203, https://doi.org/10.1021/acs.jpcc.7b03673.

[35] S. Ishimaru, R. Shiratsuchi, G. Nogami, Pulsed electroreduction of CO 2 on Cu-Ag alloy electrodes, J. Electrochem. Soc. 147 (2000) 1864, https://doi.org/10.1149/1.1393448.

[36] T.T.H. Hoang, S. Verma, S. Ma, T.T. Fister, J. Timoshenko, A.I. Frenkel, P.J. A. Kenis, A.A. Gewirth, Nanoporous copper–silver alloys by additive-controlled electrodeposition for the selective electroreduction of CO2 to ethylene and ethanol, J. Am. Chem. Soc. 140 (2018) 5791–5797, https://doi.org/10.1021/jacs.8b01868.

[37] Y. Mun, S. Lee, A. Cho, S. Kim, J.W. Han, J. Lee, Cu-Pd alloy nanoparticles as highly selective catalysts for efficient electrochemical reduction of CO2 to CO, Appl. Catal. B 246 (2019) 82–88, https://doi.org/10.1016/j.apcatb.2019.01.021.

[38] E. Torralba, N. Blanchard, C. Cachet-Vivier, D. Muller-Bouvet, J. González, S. Bastide, Electrochemical study of carbon dioxide reduction at copper–palladium nanoparticles: influence of the bimetallic composition in the CO poisoning tolerance, Electrochim. Acta 354 (2020), 136739, https://doi.org/10.1016/j.electacta.2020.136739.

[39] A. Saxena, W. Liyanage, J. Masud, S. Kapila, M. Nath, Selective electroreduction of CO 2 to carbon-rich products with a simple binary copper selenide electrocatalyst, J. Mater. Chem. A 9 (2021) 7150–7161, https://doi.org/10.1039/D0TA11518E.

[40] S. Mezzavilla, Y. Katayama, R. Rao, J. Hwang, A. Regoutz, Y. Shao-Horn, I. Chorkendorff, I.E.L. Stephens, Activity–or lack thereof–of RuO2-based electrodes in the electrocatalytic reduction of CO2, J. Phys. Chem. C. 123 (2019) 17765–17773, https://doi.org/10.1021/acs.jpcc.9b01431.

[41] A. Bandi, Electrochemical reduction of carbon dioxide on conductive metallic oxides, J. Electrochem. Soc. 137 (1990) 2157, https://doi.org/10.1149/1.2086903.

[42] C.-.W. Kung, C.O. Audu, A.W. Peters, H. Noh, O.K. Farha, J.T. Hupp, Copper nanoparticles installed in metal–organic framework thin films are electrocatalytically competent for CO2 reduction, ACS Energy Lett. 2 (2017) 2394–2401, https://doi.org/10.1021/acsenergylett.7b00621.

[43] Z. Sun, T. Ma, H. Tao, Q. Fan, B. Han, Fundamentals and challenges of electrochemical CO2 reduction using two-dimensional materials, Chem 3 (2017) 560–587, https://doi.org/10.1016/j.chempr.2017.09.009.

[44] K. Sonoda, M. Yamamoto, T. Tanabe, T. Yoshida, Synthesis of α-Ga2O3 by water oxidation of metallic gallium as a photocatalyst for CO2 reduction with water, ACS Omega 6 (2021) 18876–18880, https://doi.org/10.1021/acsomega.1c02088.

[45] C. Lamy, S. Rousseau, E.M. Belgsir, C. Coutanceau, J.-.M. Léger, Recent progress in the direct ethanol fuel cell: development of new platinum–tin electrocatalysts, Electrochim. Acta 49 (2004) 3901–3908, https://doi.org/10.1016/j.electacta.2004.01.078.

[46] D. Karapinar, C.E. Creissen, J.G. Rivera de la Cruz, M.W. Schreiber, M. Fontecave, Electrochemical CO2 reduction to ethanol with copper-based catalysts, ACS Energy Lett. 6 (2021) 694–706, https://doi.org/10.1021/acsenergylett.0c02610.

[47] Q. Li, J. Fu, W. Zhu, Z. Chen, B. Shen, L. Wu, Z. Xi, T. Wang, G. Lu, J.-.J. Zhu, S. Sun, Tuning Sn-catalysis for electrochemical reduction of CO2 to CO via the Core/Shell Cu/SnO2 structure, J. Am. Chem. Soc. 139 (2017) 4290–4293, https://doi.org/10.1021/jacs.7b00261.

[48] C. Wu, B.P. Mosher, T. Zeng, One-step green route to narrowly dispersed copper nanocrystals, J. Nanopart. Res. 8 (2006) 965–969, https://doi.org/10.1007/s11051-005-9065-2.

[49] T.M.D. Dang, T.T.T. Le, E. Fribourg-Blanc, M.C. Dang, The influence of solvents and surfactants on the preparation of copper nanoparticles by a chemical reduction method, Adv. Nat. Sci: Nanosci. Nanotechnol. 2 (2011), 025004, https://doi.org/10.1088/2043-6262/2/2/025004.

[50] X. Cheng, X. Zhang, H. Yin, A. Wang, Y. Xu, Modifier effects on chemical reduction synthesis of nanostructured copper, Appl. Surf. Sci. 253 (2006) 2727–2732, https://doi.org/10.1016/j.apsusc.2006.05.125.

[51] S.-.H. Wu, D.-.H. Chen, Synthesis of high-concentration Cu nanoparticles in aqueous CTAB solutions, J. Colloid Interface Sci. 273 (2004) 165–169, https://doi.org/10.1016/j.jcis.2004.01.071.

[52] A. Bisht, P. Zhang, C. Shivakumara, S. Sharma, Activity of Pt4+ towards the CO poisoning effect in formic acid and methanol electro-oxidation compared to Pt metal, J. Phys. Chem. (2015) 34.

[53] R. Wang, R. Jiang, C. Dong, T. Tong, Z. Li, H. Liu, X.-.W. Du, Engineering a Cu/ZnOx interface for high methane selectivity in CO2 electrochemical reduction, Ind. Eng. Chem. Res. 60 (2021) 273–280, https://doi.org/10.1021/acs.iecr.0c04718.

[54] Q. Zhang, K. Zhang, D. Xu, G. Yang, H. Huang, F. Nie, C. Liu, S. Yang, CuO nanostructures: synthesis, characterization, growth mechanisms, fundamental properties, and applications, Prog. Mater Sci. 60 (2014) 208–337, https://doi.org/10.1016/j.pmatsci.2013.09.003.

[55] M.E. Grigore, E.R. Biscu, A.M. Holban, M.C. Gestal, A.M. Grumezescu, Methods of synthesis, properties and biomedical applications of CuO nanoparticles, Pharmaceuticals (Basel) 9 (2016) E75, https://doi.org/10.3390/ph9040075.

[56] J. Jayaprakash, N. Srinivasan, P. Chandrasekaran, Surface modifications of CuO nanoparticles using Ethylene diamine tetra acetic acid as a capping agent by sol-gel routine, Spectrochim. Acta A Mol. Biomol. Spectrosc. 123 (2014) 363–368, https://doi.org/10.1016/j.saa.2013.12.080.

[57] Y.-.F. Lim, C.S. Chua, C.J.J. Lee, D. Chi, Sol–gel deposited Cu2O and CuO thin films for photocatalytic water splitting, Phys. Chem. Chem. Phys. 16 (2014) 25928–25934, https://doi.org/10.1039/C4CP03241A.

[58] L.L. Hench, J.K. West, The sol-gel process, Chem. Rev. 90 (1990) 33–72, https://doi.org/10.1021/cr00099a003.

[59] D. Ren, B.S.-H. Ang, B.S. Yeo, Tuning the selectivity of carbon dioxide electroreduction toward ethanol on oxide-derived CuxZn catalysts, ACS Catal. 6 (2016) 8239–8247, https://doi.org/10.1021/acscatal.6b02162.

[60] W. Zhu, K. Zhao, S. Liu, M. Liu, F. Peng, P. An, B. Qin, H. Zhou, H. Li, Z. He, Low-overpotential selective reduction of CO2 to ethanol on electrodeposited CuxAuy nanowire arrays, J. Energy Chem. 37 (2019) 176–182, https://doi.org/10.1016/j.jechem.2019.03.030.

[61] F. Yu, F. Li, B. Zhang, H. Li, L. Sun, Efficient electrocatalytic water oxidation by a copper oxide thin film in borate buffer, ACS Catal. 5 (2015) 627–630, https://doi.org/10.1021/cs501510e.

[62] J. Du, Z. Chen, S. Ye, B.J. Wiley, T.J. Meyer, Copper as a robust and transparent electrocatalyst for water oxidation, Angew. Chem. Int. Ed. 54 (2015) 2073–2078, https://doi.org/10.1002/anie.201408854.

[63] J. Sultana, S. Paul, A. Karmakar, G.K. Dalapati, S. Chattopadhyay, Optimizing the thermal annealing temperature: technological route for tuning the photo-detecting property of p-CuO thin films grown by chemical bath deposition method, J. Mater. Sci. Mater. Electron. 29 (2018) 12878–12887, https://doi.org/10.1007/s10854-018-9407-3.

[64] C.W. Li, M.W. Kanan, CO2 reduction at low overpotential on Cu electrodes resulting from the reduction of thick Cu2O films, J. Am. Chem. Soc. 134 (2012) 7231–7234, https://doi.org/10.1021/ja3010978.

[65] A. Verdaguer-Casadevall, C.W. Li, T.P. Johansson, S.B. Scott, J.T. McKeown, M. Kumar, I.E.L. Stephens, M.W. Kanan, I. Chorkendorff, Probing the active surface sites for CO reduction on oxide-derived copper electrocatalysts, J. Am. Chem. Soc. 137 (2015) 9808–9811, https://doi.org/10.1021/jacs.5b06227.

[66] S.B. Scott, T.V. Hogg, A.T. Landers, T. Maagaard, E. Bertheussen, J.C. Lin, R. C. Davis, J.W. Beeman, D. Higgins, W.S. Drisdell, C. Hahn, A. Mehta, B. Seger, T. F. Jaramillo, I. Chorkendorff, Absence of oxidized phases in Cu under CO reduction conditions, ACS Energy Lett. 4 (2019) 803–804, https://doi.org/10.1021/acsenergylett.9b00172.

[67] A. Paracchino, V. Laporte, K. Sivula, M. Grätzel, E. Thimsen, Highly active oxide photocathode for photoelectrochemical water reduction, Nat. Mater. 10 (2011) 456–461, https://doi.org/10.1038/nmat3017.

[68] D. Zhong, Z.-.J. Zhao, Q. Zhao, D. Cheng, B. Liu, G. Zhang, W. Deng, H. Dong, L. Zhang, J. Li, J. Li, J. Gong, Coupling of Cu(100) and (110) facets promotes carbon dioxide conversion to hydrocarbons and alcohols, Angew. Chem. Int. Ed. 60 (2021) 4879–4885, https://doi.org/10.1002/anie.202015159.

[69] B. Liu, X. Yao, Z. Zhang, C. Li, J. Zhang, P. Wang, J. Zhao, Y. Guo, J. Sun, C. Zhao, Synthesis of Cu2O nanostructures with tunable crystal facets for electrochemical CO2 reduction to alcohols, ACS Appl. Mater. Interfaces. 13 (2021) 39165–39177, https://doi.org/10.1021/acsami.1c03850.

[70] J. VandeVondele, M. Krack, F. Mohamed, M. Parrinello, T. Chassaing, J. Hutter, Quickstep: fast and accurate density functional calculations using a mixed Gaussian and plane waves approach, Comput. Phys. Commun. 167 (2005) 103–128, https://doi.org/10.1016/j.cpc.2004.12.014.

[71] J. Hutter, M. Iannuzzi, F. Schiffmann, J. VandeVondele, cp2k: atomistic simulations of condensed matter systems, WIREs Comput. Mol. Sci. 4 (2014) 15–25, https://doi.org/10.1002/wcms.1159.

[72] J.P. Perdew, K. Burke, M. Ernzerhof, Generalized gradient approximation made simple, Phys. Rev. Lett. 77 (1996) 3865–3868, https://doi.org/10.1103/PhysRevLett.77.3865.

[73] K.R. Hahn, M. Iannuzzi, A.P. Seitsonen, J. Hutter, Coverage effect of the CO2 adsorption mechanisms on CeO2(111) by first principles analysis, J. Phys. Chem. C. 117 (2013) 1701–1711, https://doi.org/10.1021/jp309565u.

[74] S. Wang, J. Wang, H. Xin, Insights into electrochemical CO2 reduction on tin oxides from first-principles calculations, Green Energy Environ. 2 (2017) 168–171, https://doi.org/10.1016/j.gee.2017.02.005.

[75] J. VandeVondele, J. Hutter, Gaussian basis sets for accurate calculations on molecular systems in gas and condensed phases, J. Chem. Phys. 127 (2007), 114105, https://doi.org/10.1063/1.2770708.

[76] S. Goedecker, M. Teter, J. Hutter, Separable dual-space Gaussian pseudopotentials, Phys. Rev. B. 54 (1996) 1703–1710, https://doi.org/10.1103/PhysRevB.54.1703.

[77] S. Grimme, J. Antony, S. Ehrlich, H. Krieg, A consistent and accurate ab initio parametrization of density functional dispersion correction (DFT-D) for the 94 elements H-Pu, J. Chem. Phys. 132 (2010), 154104, https://doi.org/10.1063/1.3382344.

[78] P. Bera, K.R. Priolkar, P.R. Sarode, M.S. Hegde, S. Emura, R. Kumashiro, N.P. Lalla, Structural investigation of combustion synthesized Cu/CeO2 catalysts by EXAFS and other physical techniques: formation of a Ce1-xCuxO2-δ solid solution, Chem. Mater. 14 (2002) 3591–3601, https://doi.org/10.1021/cm0201706.

[79] N. Sethulakshmi, S. Nellaiappan, P. Pentyala, M. Sharma, S. Irusta, P. A. Deshpande, S. Sharma, Nanocoral CuCo2S4 thiospinels: oxygen evolution reaction via redox interaction of metal ions, Electrochim. Acta 370 (2021), 137701, https://doi.org/10.1016/j.electacta.2020.137701.

[80] S. Nitopi, E. Bertheussen, S.B. Scott, X. Liu, A.K. Engstfeld, S. Horch, B. Seger, I.E. L. Stephens, K. Chan, C. Hahn, J.K. Nørskov, T.F. Jaramillo, I. Chorkendorff, Progress and perspectives of electrochemical CO2 reduction on copper in aqueous electrolyte, Chem. Rev. 119 (2019) 7610–7672, https://doi.org/10.1021/acs.chemrev.8b00705.

[81] J.Y. Kim, G. Kim, H. Won, I. Gereige, W.-.B. Jung, H.-.T. Jung, Synergistic Effect of Cu2O Mesh Pattern on High-Facet Cu Surface for Selective CO2 electroreduction to ethanol, Adv. Mater. n/a 34 (2022), 2106028, https://doi.org/10.1002/adma.202106028.

[82] K. Zhao, Y. Liu, X. Quan, S. Chen, H. Yu, CO2 electroreduction at low overpotential on oxide-derived Cu/carbons fabricated from metal organic framework, ACS Appl. Mater. Interfaces. 9 (2017) 5302–5311, https://doi.org/10.1021/acsami.6b15402.

[83] H. Jung, S.Y. Lee, C.W. Lee, M.K. Cho, D.H. Won, C. Kim, H.-.S. Oh, B.K. Min, Y. J. Hwang, Electrochemical fragmentation of Cu2O nanoparticles enhancing selective C–C coupling from CO2 reduction reaction, J. Am. Chem. Soc. 141 (2019) 4624–4633, https://doi.org/10.1021/jacs.8b11237.

[84] A.D. Handoko, C.W. Ong, Y. Huang, Z.G. Lee, L. Lin, G.B. Panetti, B.S. Yeo, Mechanistic insights into the selective electroreduction of carbon dioxide to ethylene on Cu2O-derived copper catalysts, J. Phys. Chem. C. 120 (2016) 20058–20067, https://doi.org/10.1021/acs.jpcc.6b07128.

[85] L. Qi, S. Liu, W. Gao, Q. Jiang, Mechanistic understanding of CO2 electroreduction on Cu2O, J. Phys. Chem. C. 122 (2018) 5472–5480, https://doi.org/10.1021/acs.jpcc.7b11842.

[86] D. Ren, Y. Deng, A.D. Handoko, C.S. Chen, S. Malkhandi, B.S. Yeo, Selective electrochemical reduction of carbon dioxide to ethylene and ethanol on copper(I) oxide catalysts, ACS Catal. 5 (2015) 2814–2821, https://doi.org/10.1021/cs502128q.

[87] J.K. Nørskov, F. Studt, F. Abild-Pedersen, T. Bligaard. Fundamental Concepts in Heterogeneous Catalysis, 2014, p. 208.

[88] M. Che, Nobel Prize in chemistry 1912 to Sabatier: organic chemistry or catalysis? Catal. Today 218–219 (2013) 162–171, https://doi.org/10.1016/j.cattod.2013.07.006.

[89] Y. Duan, K. Zhang, X. Xie, Theoretical studies of CO and NO on CuO and Cu2O (110) surfaces, Surface Sci. 321 (1994) L249–L254, https://doi.org/10.1016/0039-6028(94)90183-X.

[90] T.-.T. Zhuang, Z.-.Q. Liang, A. Seifitokaldani, Y. Li, P. De Luna, T. Burdyny, F. Che, F. Meng, Y. Min, R. Quintero-Bermudez, C.T. Dinh, Y. Pang, M. Zhong, B. Zhang, J. Li, P.-.N. Chen, X.-.L. Zheng, H. Liang, W.-.N. Ge, B.-.J. Ye, D. Sinton, S.-.H. Yu, E. H. Sargent, Steering post-C–C coupling selectivity enables high efficiency electroreduction of carbon dioxide to multi-carbon alcohols, Nat. Catal. 1 (2018) 421–428, https://doi.org/10.1038/s41929-018-0084-7.

[91] K. Jiang, R.B. Sandberg, A.J. Akey, X. Liu, D.C. Bell, J.K. Nørskov, K. Chan, H. Wang, Metal ion cycling of Cu foil for selective C–C coupling in electrochemical CO2 reduction, Nat. Catal. 1 (2018) 111–119, https://doi.org/10.1038/s41929-017-0009-x.

[92] K.J.P. Schouten, Y. Kwon, C.J.M. van der Ham, Z. Qin, M.T.M. Koper, A new mechanism for the selectivity to C1 and C2 species in the electrochemical reduction of carbon dioxide on copper electrodes, Chem. Sci. 2 (2011) 1902–1909, https://doi.org/10.1039/C1SC00277E.

[93] R. Kortlever, J. Shen, K.J.P. Schouten, F. Calle-Vallejo, M.T.M. Koper, Catalysts and reaction pathways for the electrochemical reduction of carbon dioxide, J. Phys. Chem. Lett. 6 (2015) 4073–4082, https://doi.org/10.1021/acs.jpclett.5b01559.